

# A Novel High-Performance Magnetic Gear

K. Atallah and D. Howe

**Abstract**—Mechanical gearboxes are used extensively to match the operating speed of prime-movers to the requirements of their loads. Although, high system torque densities can be achieved, gear lubrication and cooling are often required, whilst noise, vibration and reliability can be significant issues. The paper describes the design and performance of a magnetic gear, which employs rare-earth magnets, which simulation studies have shown to have a transmitted torque density exceeding  $100 \text{ kNm/m}^3$ .

**Index Terms**—Gearboxes, gears, magnetic circuits.

## I. INTRODUCTION

**M**ECHANICAL gearboxes are used extensively to match the operating speed of prime-movers to the requirements of their loads, both for increasing the rotational speed (e.g., windmill-powered generators) and decreasing the speed (e.g., electric-ship propulsion), since it is usually more cost and weight effective to employ a high-speed electrical machine together with a gearbox to transform speed and torque. However, although, high system torque densities can then be achieved, gear lubrication and cooling are often required, whilst noise, vibration and reliability can be significant issues. In contrast, magnetic gearing has received relatively little attention, probably because of the relative complexity and poor torque density of the magnetic circuits which have been proposed [1], [2]. For applications in which mechanical gearing cannot be accommodated, direct electrical drives must be employed. Of the various competing direct drive machine topologies, permanent magnet transverse-field machines offer potentially the highest torque densities [3], [4], typically in the range  $40\text{--}80 \text{ kNm/m}^3$ . However, since they have an inherently poor power factor, they are inappropriate for electrical power generation applications, and require a significantly higher converter volt-ampere rating for motoring applications than conventional permanent magnet brushless machines. The paper describes the design and performance of a magnetic gear, which employs rare-earth magnets, which simulation studies have shown to have a transmitted torque density capability which is comparable with that of two- and three-stage helical gearboxes, *viz.*  $50\text{--}150 \text{ kNm/m}^3$ . When combined with a conventional topology of permanent magnet brushless machine, such a magnetic gearbox could offer significant advantages in applications as diverse as embedded motor/generator units in more-electric aircraft engines, electric ship propulsion, wind power generation etc.

Manuscript received October 13, 2000.

The authors are with the Department of Electronic and Electrical Engineering, The University of Sheffield, Sheffield S1 3JD, England (e-mail: k.atallah@sheffield.ac.uk).

Publisher Item Identifier S 0018-9464(01)07092-3.

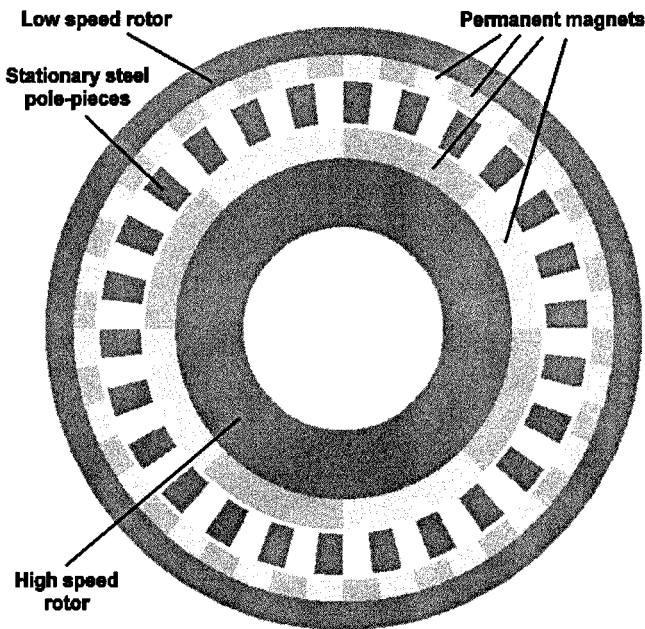


Fig. 1. Schematic of magnetic gear.

## II. PRINCIPLE OF OPERATION

Fig. 1 shows a schematic of the proposed magnetic gear topology. It can be shown that the number of pole-pairs in the space harmonic flux density distribution produced by either the high or low speed rotor permanent magnets, is given by:

$$\begin{aligned} p_{m,k} &= |mp + kn_s| \\ m &= 1, 3, 5, \dots, \infty \\ k &= 0, \pm 1, \pm 2, \pm 3, \dots, \pm \infty \end{aligned} \quad (1)$$

where  $p$  is the number of pole-pairs on permanent magnet rotor, and  $n_s$  the number of stationary steel pole-pieces. Furthermore, the rotational velocity of the flux density space harmonics is given by:

$$\Omega_{m,k} = \frac{mp}{mp + kn_s} \Omega_r \quad (2)$$

where  $\Omega_r$  is the rotational velocity of the permanent magnet rotor. From (2), it can be seen that the velocity of the space harmonics due to the introduction of the steel pole-pieces, *viz.*  $k \neq 0$ , is different to the velocity of the rotor which carries the permanent magnets. Therefore, in order to transmit torque at a different speed, the number of pole-pairs of the other permanent magnet rotor must be equal to the number of pole-pairs of a space harmonic for which  $k \neq 0$ . The gear ratio is then given by:

$$G_r = \frac{mp}{|mp + kn_s|} \quad (3)$$

TABLE I  
PARAMETERS OF MAGNETIC GEAR

Parameter	
Number of pole-pairs on high speed rotor	$p_h = 4$
Number of pole-pairs on low speed rotor	$p_l = 22$
Number of stationary steel pole-pieces	$n_s = 26$
Airgap length	1 mm
Outside diameter	140 mm
Remanence of sintered NdFeB	$B_r = 1.25$ T
Relative recoil permeability of sintered NdFeB	$\mu_r = 1.05$
Grade of silicon steel laminations	A300-35

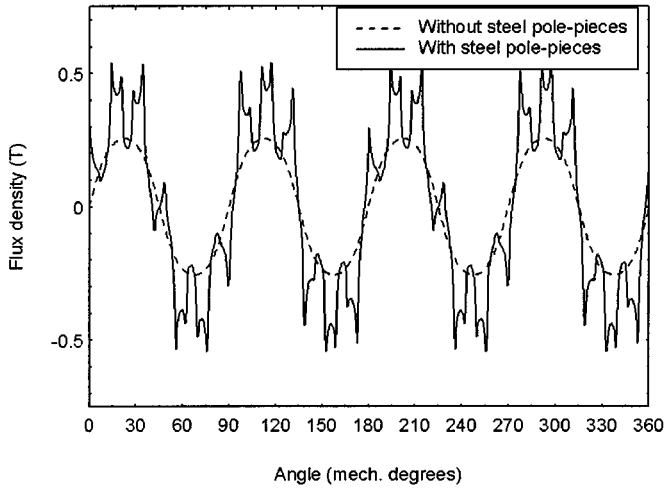


Fig. 2. Variation of radial flux density, due to high speed permanent magnet rotor, in airgap adjacent to low speed rotor.

### III. SIMULATION STUDIES

Two-dimensional magnetostatic finite element method was employed for the simulation studies. Table I gives the parameters which have been assumed for the magnetic gear, shown in Fig. 1. Both the high and low speed rotors being equipped with sintered NdFeB permanent magnets, and the steel pole-pieces and the rotors cores being made of silicon steel laminations.

#### A. Flux Density Distributions

Fig. 2 shows the variation of the radial component of flux density due to the high speed rotor permanent magnets in the airgap adjacent to the low speed rotor, whilst Fig. 3 shows the corresponding space harmonic spectrum. It can be seen that the presence of the steel pole-pieces results in a number of asynchronous, *viz.*  $k \neq 1$ , space harmonics, the largest of which is the 22 pole-pair space harmonic, ( $m = 1, k = -1$ ), which interacts with the 22 pole-pair low speed rotor permanent magnets to transmit a torque at a rotational velocity of:

$$\Omega_l = \frac{p_h}{p_h - n_s} \Omega_h = -\frac{1}{5.5} \Omega_h \quad (4)$$

where  $\Omega_h$  and  $\Omega_l$  are the rotational velocities of the high and low speed rotors, respectively.

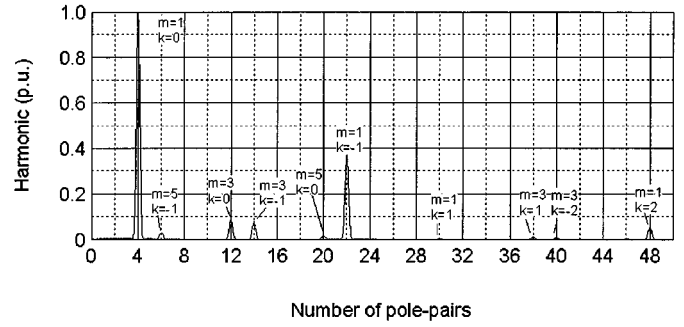


Fig. 3. Space harmonic spectrum of radial flux density, due to the high speed permanent magnet rotor, in airgap adjacent to low speed rotor.

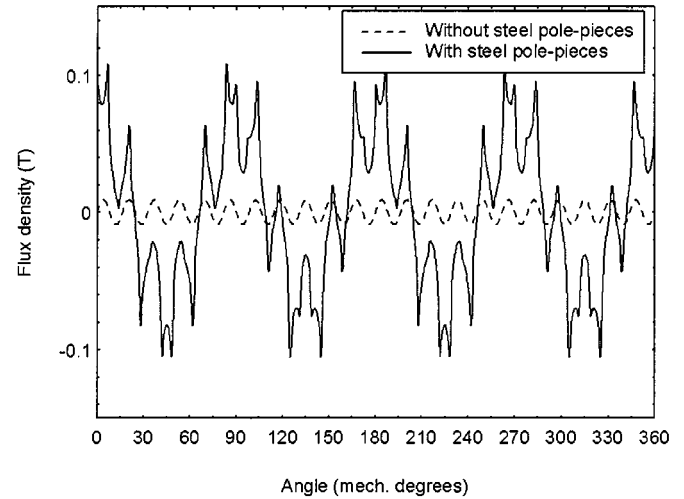


Fig. 4. Variation of radial flux density, due to low speed permanent magnet rotor, in airgap adjacent to high speed rotor.

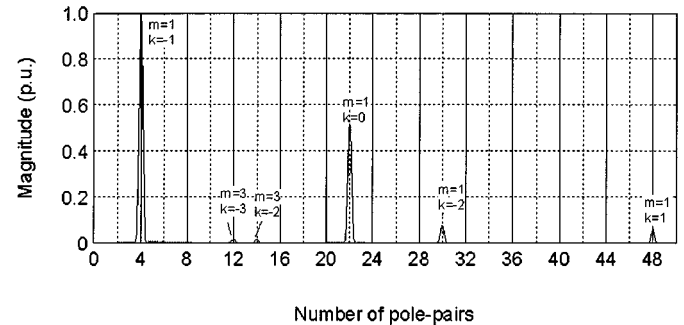


Fig. 5. Space harmonic spectrum of radial flux density, due to low speed permanent magnet rotor, in airgap adjacent to high speed rotor.

Similarly, Fig. 4 shows the variation of the radial component of flux density due to the low speed rotor permanent magnets in the airgap adjacent to the high speed rotor, whilst Fig. 5 shows the corresponding space harmonic spectrum. It can be seen that the presence of the steel pole-pieces results in a dominant 4 pole-pair asynchronous space harmonic, ( $m = 1, k = -1$ ), which interacts with the 4 pole-pair high speed rotor permanent magnets to transmit torque at a rotational velocity of:

$$\Omega_h = \frac{p_l}{p_l - n_s} \Omega_l = -5.5 \Omega_l \quad (5)$$

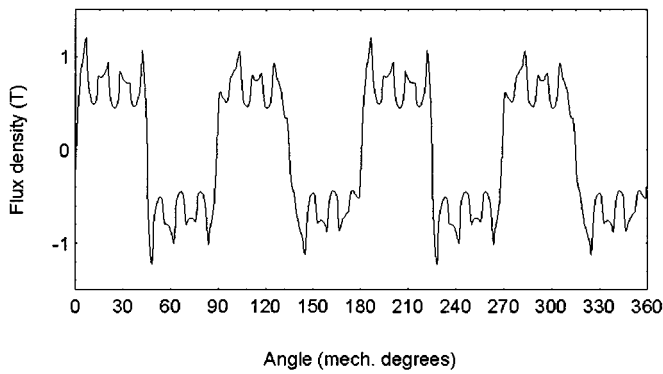


Fig. 6. Variation of radial component of resultant fluxdensity in airgap adjacent to high speed rotor.

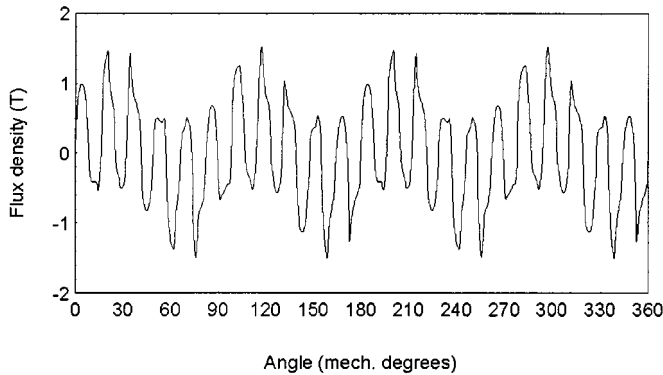


Fig. 7. Variation of radial component of resultant flux density in airgap adjacent to low speed rotor.

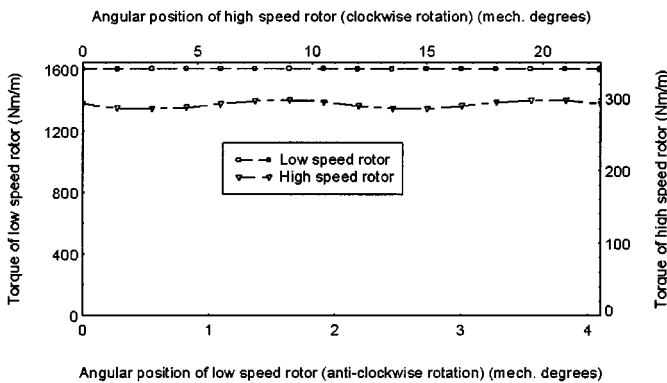


Fig. 8. Variation of maximum torque on low and high speed rotors.

Figs. 6 and 7 show the variation of the radial component of the resultant flux density, due to both permanent magnet rotors, in the airgaps adjacent to the high and low speed rotors, respectively.

### B. Torque Transmission

Fig. 8 shows the variation of the maximum torque which is exerted on the high and low speed rotors as they rotate. As can be seen, a transmitted torque density exceeding  $100 \text{ kNm/m}^3$  can be achieved. Fig. 9 shows how the system torque density of a combined magnetic gear and permanent magnet brushless machine varies with the gear ratio and the torque density of the machine,  $10 \text{ kNm/m}^3$ ,  $20 \text{ kNm/m}^3$  and  $30 \text{ kNm/m}^3$  being typical

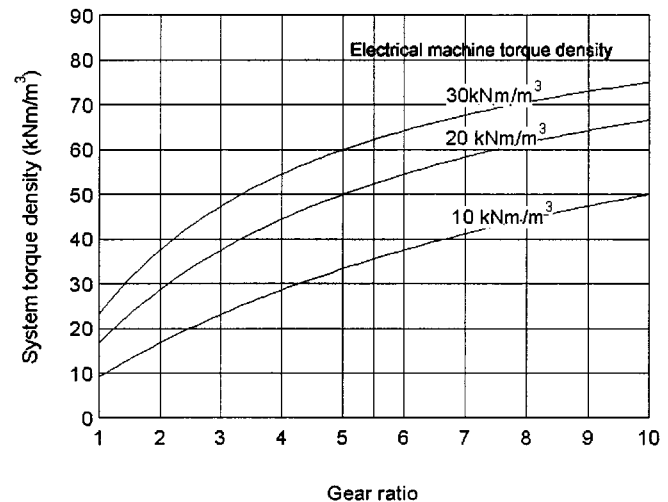


Fig. 9. Variation of system torque density with gear ratio for different electrical machine torque densities (magnetic gear torque density is  $100 \text{ kNm/m}^3$ ).

for naturally-cooled, forced air-cooled and liquid-cooled radial field permanent magnet brushless motors, respectively. As can be seen, a system torque density which is comparable or better than that of a state-of-the-art transverse-field machine can be achieved by employing a gear ratio between 5–10 and a conventional radial-field machine topology, with the attendant benefits which this brings in terms of manufacturing simplicity, improved power factor etc.

In addition to mechanical losses, *viz.* bearing friction and rotor windage, a magnetic gear will have two electromagnetic loss components, *viz.*

- Iron loss in the laminated back-iron of both rotors and the stationary laminated steel pole-pieces.
- Induced eddy current loss in the rotor permanent magnets.

Further simulation studies are being carried out to evaluate the effect of these on the efficiency and thermal performance of the proposed magnetic gear.

### IV. CONCLUSIONS

A novel topology for a high-performance magnetic gear has been presented. It has been shown that, by employing rare-earth magnets, a torque density exceeding  $100 \text{ kNm/m}^3$  can be achieved. It has also been shown that the system (*i.e.*, magnetic gear and electrical machine) torque density can be comparable or better than that of a transverse-field machine.

### REFERENCES

- [1] D. E. Hesmondhalgh and D. Tipping, "A multielement magnetic gear," *IEE Proceedings*, pt. B, vol. 127, pp. 129–138, 1980.
- [2] K. Tsurumoto and S. Kikushi, "A new magnetic gear using permanent magnet," *IEEE Transactions on Magnetics*, vol. MAG-23, no. 5, pp. 3622–3624, 1987.
- [3] M. R. Harris, G. H. Pajooman, and S. M. Abu Sharkh, "Performance and design optimization of electric motors with heteropolar surface magnets and homopolar windings," *IEE Proceedings*, pt. B, vol. 143, no. 6, pp. 429–436, 1996.
- [4] H. Weh, "Transverse flux (TF) machines in drive and generator applications," in *Proceedings of IEEE/KTH Stockholm Power Technology Conference*, Stockholm, Sweden, 1995, pp. 75–80.